

## Experimental Evidence for High-Efficiency, Low-Brightness Behavior in Free-Electron Lasers

D. Iracane, V. Fontenay, P. Guimbal, S. Joly, S. Striby, and D. Touati  
*Commissariat à l'Energie Atomique, B.P.12 91680 Bruyères-le-Châtel, France*  
 (Received 15 March 1994)

Spectral broadening is expected in free-electron lasers (FEL) due to sideband generation and nonlinear mode coupling. For high enough electron current, the FEL beam presents an asymptotic regime characterized by a broad and turbulent spectrum. Theoretical investigations have shown that this regime also exhibits a strong efficiency enhancement and a universal low brightness. This paper reports experimental evidence for these new scaling laws using the rf linac-based ELSA FEL.

PACS numbers: 41.60.Cr, 52.35.Mw, 52.35.Ra

A Compton free-electron laser (FEL) provides physics issues that are typical of a wide range of plasma physics problems where electrons and electromagnetic waves are coupled in a highly nonlinear way. Extensive numerical and theoretical investigations [1,2] lead to the following scenario for the FEL spectral behavior. Because of the synchrotron motion of the electrons, a sideband mode appears after saturation of the fundamental line [3]. Then, nonlinear mode coupling mechanisms, such as difference frequency generation [1], result in an effective efficiency enhancement to the cost of a strong broadening of the FEL spectrum. Numerical simulations exhibit a saturation of this broadening process, which we call the post-sideband regime. It is characterized by a turbulent spectrum with some stable mean values as the extraction efficiency  $\rho$  and the rms relative spectral width  $\Sigma = (\langle \omega^2 \rangle - \langle \omega \rangle^2)^{1/2} / \langle \omega \rangle$ . Moreover, it appears that the scaled brightness defined as  $\beta = \rho / \Sigma$  is approximately 0.8 for a wide range of FEL parameters [1], as long as lasing is in the postsideband regime. To explain this, a new saturation mechanism was proposed [2]: A stochastic description of the chaotic electron dynamics under the influence of a broad FEL spectrum leads to a diffusion equation for the electron energy. The diffusion coefficient is proportional to the spectral density and the electrons spread over a phase space area strictly related to the spectral width. The brightness deduced from this assumption is  $\beta = \sqrt{3}/2$ , in good agreement with simulations.

It was necessary to validate these results by experiments. First, simulations may exhibit spurious chaotic behaviors due to numerical noise generation or poor statistics. Second, the random phase approximation used in the model [2] needs to be tested in the strong mode coupling regime, beyond the scope of standard quasilinear theory.

Although the chaotic behavior in the broad spectrum regime has been widely reported [4], no quantitative analysis of the spectral width and of the efficiency was provided. Moreover, a few FEL devices can be used to investigate these postsideband regimes which require not only high-electron currents but also long-pulse capabilities to reach the steady state; therefore the ELSA FEL is

well suited to perform the relevant experiments.

The ELSA facility is an oscillator FEL [5,6] using a rf accelerator and currently producing a tunable laser beam in the 18 to 40  $\mu\text{m}$  range. Low emittance, high charge electron bunches are produced by a 144 MHz photoelectric injector and accelerated by 433 MHz cavities to a maximum energy of 18 MeV. Because of the long macropulse duration (up to 160  $\mu\text{s}$ , i.e., 2300 round trips), issues related to high-power FEL's can be addressed. Data reported below were obtained with 50  $\mu\text{s}$  long macropulses which are long enough to reach a steady state (the rise time of the signal is less than 5  $\mu\text{s}$ ). A photoinjector offers a great flexibility for adjusting the main parameters controlling beam emittance. The drive laser pulse had a diameter on cathode of 4 mm and a longitudinal Gaussian shape (20 ps FWHM). With these laser initial conditions, we measured a transverse normalized rms emittance of  $3\pi$  mmmrad at the linac exit for 16.5 MeV, 1.0 nC bunches. The experiments have been performed in these conditions. Amplitude and phase fluctuations within the macropulse have been reduced using feedforward and feedback loop systems: rms phase jitters are lower than  $0.1^\circ$  and rms amplitude fluctuations smaller than 0.1%. Measurements with a synchroscan streak camera showed the rms phase jitter between micropulses was below 3 ps.

The macropulse FEL spectrum is analyzed by a 0.32 m monochromator coupled with a 512-element pyroelectric array detector; the measured resolution is about 12 nm at 20  $\mu\text{m}$  and the covered spectral range is about 13%. After calibration,  $\Sigma$  is directly deduced from the digitized data. In the 20  $\mu\text{m}$  region, the raw spectra are spoiled by water absorption lines (see Fig. 1), but this has a slight effect on  $\Sigma$ . As the macropulse is quite long compared to the transient regimes,  $\Sigma$  can be gauged on a spectrum integrated over the macropulse rather than on an instantaneous spectrum at saturation. This leads to an accuracy of about 5%.

At saturation,  $\rho$  is equal to the relative energy loss of the electron beam through the wiggler. To get an absolute value for  $\rho$ , we use an optical transition radiation screen set in the focal plane of a  $150^\circ$  magnetic spectrometer. Its image is acquired on a charge-coupled de-

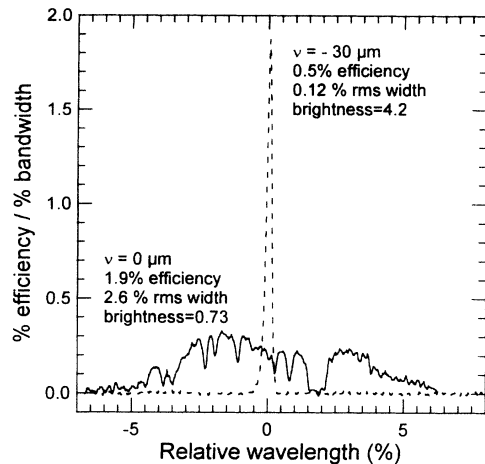


FIG. 1. Two centered FEL spectra illustrating typical regimes depending on the cavity detuning  $\nu$ .

vice (CCD) camera after reflecting from a 1500 rpm spinning mirror to provide the evolution of the electron spectrum during the macropulse with a  $2 \mu\text{s}$  time resolution. By switching the laser off, one obtains the initial average energy and energy spread for each micropulse within the macropulse. While lasing, the efficiency is readily obtained as the relative difference between the average electron energy at the beginning and at the end of the macropulse.

This electron diagnostic cannot be used in every run. An alternative efficiency  $\rho$  was calculated as the ratio of the extracted laser energy to the electron energy. The latter is measured with a Faraday cup for the bunch charge and from beam transport parameters for the beam kinetic energy. The mean photon micropulse energy is deduced from the total macropulse energy as given by a joulemeter and from the optical macropulse length. This length is measured with a fast HgCdTe detector having a 20 ns response time. We have computed the ratio  $R_{\text{cav}}$  of the extracted laser power relative to the power produced by the FEL interaction. Simulations exhibited a low value for  $R_{\text{cav}}$  (20% at  $20 \mu\text{m}$ ), mainly due to the small diameter of the outcoupling hole (2.3 mm). This has been corroborated by comparing the predicted total losses to the measured cavity ringdown time. Finally, we have taken into account the attenuation factor  $R_{\text{trans}}$  ( $\approx \frac{1}{3}$ ) due to the KRS-5 windows in the photon transport line. The agreement between electron and optical measurements corrected by the factor  $R_{\text{trans}}R_{\text{cav}}$  has been found to be within 30%, which is consistent with the estimated uncertainties of the optical data. Yet, as electron measurements are more reliable, they are used to calibrate optical data within a 10% uncertainty.

By using this set of diagnostics, we have studied the efficiency  $\rho$ , the relative spectral width  $\Sigma$ , and the brightness  $\beta$  for different parameters. We proceeded by detuning the optical cavity length, which is expected to induce

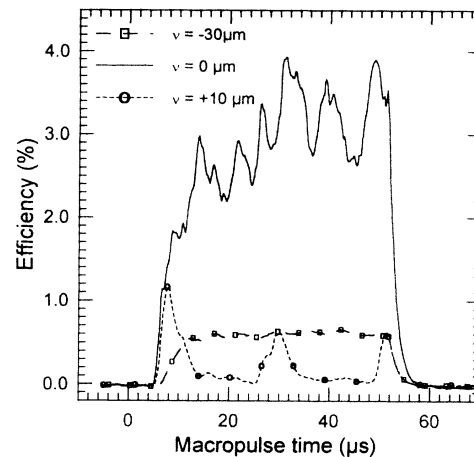


FIG. 2. Evolution of the efficiency within the macropulse for three different cavity detunings  $\nu$ . The time origin corresponds to the beginning of the drive laser macropulse.

a transition between narrow and broad spectra [4].

The standard FEL resonant condition requires, for a laser period  $\lambda_L$ , that the laser beam propagates over  $\lambda_w + \lambda_L$  when the electrons travel over one wiggler period  $\lambda_w$ . The laser advance through the wiggler is the slippage distance  $s = N_w \lambda_L$ . The physics depends on the comparison between  $s$  and  $L_p$ , where  $L_p$  is the micropulse length. When  $s \approx L_p$ , we get the superradiance regime which is beyond the scope of this paper. However, when  $s \ll L_p$ , the behavior is close to the continuous beam limit. In our case, the wiggler has 30 periods of 3.2 cm so that  $\lambda_L \approx 20 \mu\text{m}$  and  $s \approx 0.6 \text{ mm}$  is to be compared with  $L_p = 1 \text{ cm}$ . Therefore, the broad spectrum behavior predicted for a continuous beam should be observed in our experiment.

The cavity detuning  $\nu$  is defined as the cavity length minus some reference length. By varying  $\nu$ , one gets either narrow or large spectra. This is a finite length pulse effect since for large  $|\nu|$ , the light is pushed outside from the electron beam. By detuning the cavity length, one controls the interaction time between electrons and light, and thereby the instabilities. Zero detuning corresponds to a maximum of the longitudinal overlap and, following the continuous beam predictions, broad spectra are expected. For shorter cavity length ( $\nu < 0$ ), one obtains narrow Fourier-limited spectra. The contrast between the two spectra (Fig. 1) is large owing to the long ELSA micropulse.

The HgCdTe measurements allow a measure of the time stability within the macropulse (Fig. 2). For  $\nu = 0$ , the small signal gain ranges between 50% and 100% depending on the operating parameters. Thus, the rise time is very short compared to the macropulse length. In the saturation regime, one observes 20% fluctuations for the extracted power. In part this is due to variations of the electron beam, but simulations in the continuous beam limit also exhibit fluctuations typical of a turbulent re-

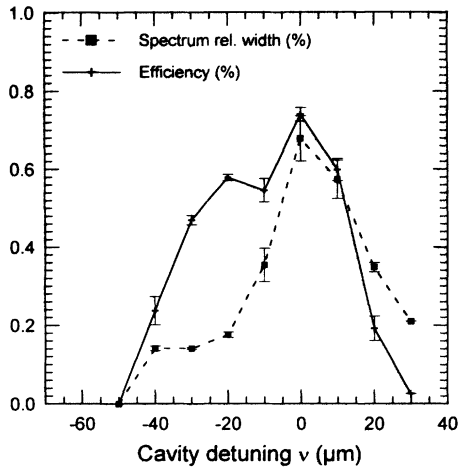


FIG. 3. Plot of the efficiency  $\rho$  and rms spectral width  $\Sigma$  versus the optical cavity detuning.

gime. For  $\nu < 0$ , one observes a low-power steady state. The situation is dramatically different for  $\nu > 0$  since the oscillations are clearly related to the dynamics. This is reproduced by numerical simulations where the signal is first amplified and then decays to the noise level, being amplified again if the macropulse is long enough. This intricate behavior may be understood by studying the weak field limit in the intermediate gain regime for a Gaussian profile of the micropulse. The manifest instability occurring at  $\nu > 0$  is also a nonlinear effect, perhaps related to the slope of the electron distribution at the central position of the laser pulse.

Figure 3 shows that the expected enhancement of the efficiency  $\rho$  for  $\nu = 0$  occurs with a strong increase of the spectral width. The scaled brightness is presented in Figs. 4(a) and 4(b) for two sets of parameters which ex-

hibit the following behavior.

(i) The brightness is equal to 0.8 as long as the efficiency is large enough. This definitively verifies the theoretical prediction of a universal brightness in the postsideband regime. Thus, for  $\nu \approx 0$ , one obtains a low-brightness, high-efficiency FEL beam.

(ii) For shorter cavity lengths ( $\nu < 0$ ), the brightness strongly increases up to 4 with a 0.5% efficiency typical of the one-frequency saturation ( $1/6N_w = 0.5\%$ ) [7], and a Fourier-limited spectral width of 0.12%. Thus, for  $\nu < 0$ , one obtains a high-brightness low-efficiency FEL beam.

(iii) We get a nonsymmetric behavior for a longer cavity length ( $\nu > 0$ ). The efficiency decreases faster than the width (see also Fig. 3). Thus, for  $\nu > 0$ , one obtains a low-brightness low-efficiency FEL beam.

The theoretical analysis proposed in Refs. [1,2] was performed by assuming a continuous beam. The longitudinal overlap at zero cavity detuning is sufficient to recover the 0.8 brightness predicted for a continuous beam. Understanding the overall experiment requires simulating finite length pulses. The synchroscan camera showed that the electron micropulse is Gaussian in longitudinal profile. Therefore, one may expect not only finite pulse effects but also pulse shape effects. For example, this shape implies that saturation occurs first at the middle of the pulse and then at the edges. Therefore, we observe the end of the linear regime 2 decades below the saturation level for a Gaussian pulse, as compared to 1 decade for a continuous beam.

Continuous beam investigation was performed using a code where the laser field is expanded as a Fourier sequence. This is the natural representation for translation invariant physics. For very short pulses, it is preferable to work in position space. For long but finite electron pulses, either of these approaches can be used. We have simulated our experiments by putting the electron and

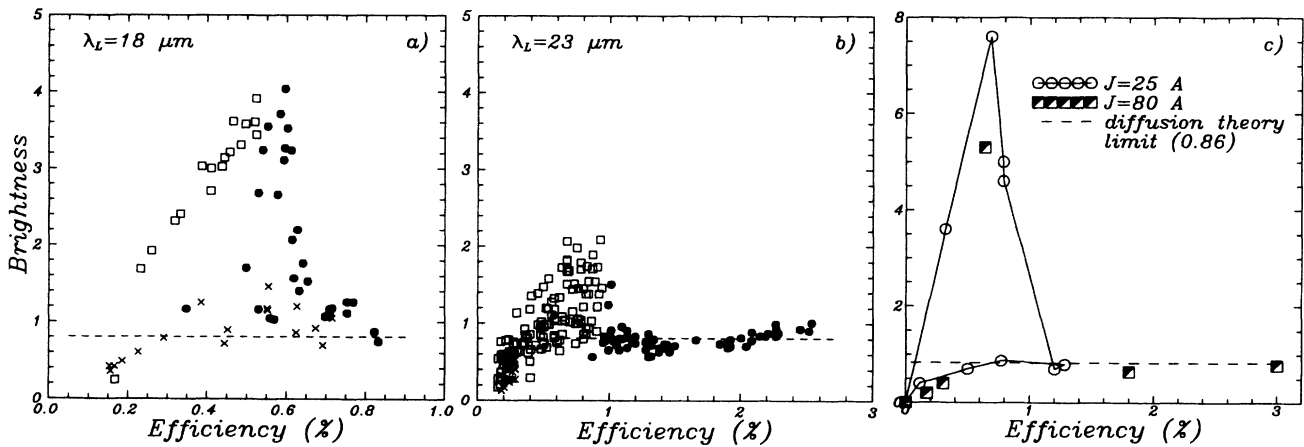


FIG. 4. Dependence of the brightness upon the efficiency. Experimental data are obtained for a low current (a) and a high current (b). The cavity length is detuned from  $\nu = -120 \mu\text{m}$  to  $40 \mu\text{m}$ . Dotted points (squared and cross points) correspond to  $-25 < \nu < 10 \mu\text{m}$  ( $\nu < -25 \mu\text{m}$  and  $\nu > 10 \mu\text{m}$ ). The behavior is accurately reproduced in simulations (c) provided for two typical beam current  $J$ .

laser beams in a periodic box. Two numerical parameters are critical: the number of laser frequencies  $N_f$  and the distance  $\delta\omega$  between two neighboring frequencies. The periodic box size  $L_B$  has to be large enough so that the laser beam is strictly included in the box; this implies  $L_B$  much larger than the sum of the electron pulse length, the slippage distance, and the cavity detuning shift. Because  $\delta\omega \approx 1/L_B$ , the number  $N_f$  is governed by the spectral width  $\Sigma$  or, equivalently, by  $\lambda_L/\Sigma$  in position space. Simulations of broad spectra and long pulses are expensive since they require a large box ( $L_B \approx 100 s$ ) and small steps in position space ( $\lambda_L/\Sigma \approx s/10$ ).

We varied the electronic peak current  $J$  by a factor 3, using a magnetic compression [8]. A rather small (high) current is used for the experiment reported in Fig. 4(a) [Fig. 4(b)]. Because precise measurements of the pulse length were not available, the simulations [Fig. 4(c)] were performed for two representative values of the current  $J$ , which led to qualitative agreement between the experiment and simulation.

Nevertheless, since the postsideband regime is robust, the 0.8 brightness for efficiencies greater than the monofrequency efficiency ( $1/6N_w$ ) is in quantitative agreement despite an overall 10% uncertainty originating mainly from the efficiency measurements. Precise knowledge of the current and the beam radius is required to improve the quantitative agreement for the lower efficiencies occurring at  $\nu < 0$  and  $\nu > 0$ .

This experimental study provides a definitive proof of

diffusionlike saturation for a high-power FEL. This work was performed with an infrared FEL. Nevertheless, the simulations and the theoretical understanding [2] of this postsideband regime allow us to assert its generality. For example, simulations performed for a FEM [9] devoted to fusion heating exhibit the same behavior and comparable mechanisms are also present in traveling wave tubes.

The authors wish to acknowledge R. Dei-Cas for his continuous encouragement and fruitful discussions.

- 
- [1] D. Iracane and J. L. Ferrer, *Phys. Rev. Lett.* **66**, 33 (1991).
  - [2] P. Chaix and D. Iracane, *Phys. Rev. E* **48**, R3259 (1993).
  - [3] N. M. Kroll, P. L. Morton, and M. N. Rosenbluth, *IEEE J. Quantum Electron.* **417**, 1436 (1981).
  - [4] R. W. Warren *et al.*, *Nucl. Instrum. Methods Phys. Res., Sect. A* **285**, 1 (1989).
  - [5] R. Dei-Cas *et al.*, *Nucl. Instrum. Methods Phys. Res., Sect. A* **318**, 121 (1992).
  - [6] S. Joly *et al.*, *Nucl. Instrum. Methods Phys. Res., Sect. A* **331**, 199 (1993).
  - [7] W. B. Colson, in *Laser Handbook: Free Electron Lasers*, edited by W. B. Colson *et al.* (North-Holland, Amsterdam, 1990).
  - [8] S. Joly *et al.*, *Nucl. Instrum. Methods Phys. Res., Sect. A* **341**, 386 (1994).
  - [9] W. H. Urbanus *et al.*, *Nucl. Instrum. Methods Phys. Res., Sect. A* **331**, 235 (1993).